# Covalently circularized nanodiscs for studying membrane proteins and viral entry

Mahmoud L Nasr[1], Diego Baptista[1], Mike Strauss[1], Zhen-Yu J Sun[1], Simina Grigoriu[1], Sonja Huser[2], Andreas Plückthun[3], Franz Hagn[4], Thomas Walz[2,5], James M Hogle[1] & Gerhard Wagner[1]

**We engineered covalently circularized nanodiscs (cNDs) which, compared with standard nanodiscs, exhibit enhanced stability, defined diameter sizes and tunable shapes. Reconstitution into cNDs enhanced the quality of nuclear magnetic resonance spectra for both VDAC-1, a β-barrel membrane protein, and the G-protein-coupled receptor NTR1, an α-helical membrane protein. In addition, we used cNDs to visualize how simple, nonenveloped viruses translocate their genomes across membranes to initiate infection.**

Phospholipid bilayer nanodiscs provide a detergent-free lipid bilayer model, enabling biochemical and biophysical characterization of membrane proteins in a physiologically relevant environment[1]. A traditional nanodisc is composed of a nanometer-sized phospholipid bilayer patch encircled by two copies of an α-helical, amphipathic membrane scaffold protein (MSP)[2,3]. MSPs are truncated forms of apolipoprotein A1 (ApoA1), which is the major protein component of high-density lipoprotein. To date, however, the utility of this system for structural studies has been limited by the heterogeneity in size and the number of membrane proteins enclosed, and only small nanodiscs can be constructed with currently available protein scaffolds[4–7].

To overcome these limitations we developed three different methods to covalently link the N and C termini of newly engineered variants based on ApoA1, and we produced nanodiscs with a large range of discrete sizes and defined geometric shapes. The protein constructs we used contained the consensus sequence recognized by sortase A (LPGTG) near the C terminus and a single glycine residue at the N terminus (**Fig. 1a** and **Supplementary Note 1**). The presence of these two sites ensures covalent linkage between the N and C termini of a protein[8] while still conserving the function to form nanodiscs.

First, we used a NanodiscWidth 11 nm (NW11) construct, which assembles an 11-nm nanodisc, to optimize protein circularization over a $Cu^{2+}$ chip (**Fig. 1b**). In this scheme, the $Cu^{2+}$ was saturated with uncircularized NW11 protein via a $His_6$ tag before evolved sortase[9] was added. Completion of these steps liberated the circularized NW11 to the solution for further purification via reverse nickel affinity chromatography. Reaction completion was confirmed by SDS–PAGE and tandem mass spectrometry (MS/MS; **Fig. 1c**,**d**). Next, using electron microscopy (EM) we confirmed that the final circularized product was still capable of assembling nanodiscs. The EM images revealed very homogenous nanodiscs, and the distribution analysis showed less variance in the diameters of cNW11 as compared with that of NW11 nanodiscs ($P < 0.001$; **Fig. 1e**). We also produced smaller cNW9 and larger cNW30 and cNW50 constructs which assemble approximately 8.5-, 15- and 50-nm nanodiscs, respectively (**Supplementary Note 1** and **Supplementary Figs. 1–4**).

Even though circularization over the surface of a $Cu^{2+}$ chip usually results in a clean final product, this approach is limited to small-scale production of circularized protein. In order to scale up the production of cNW11, we performed the circularization reaction over nickel beads (**Supplementary Fig. 5a**). To further increase the yield of cNW11, we developed a third method of performing the circularization reaction in solution (**Supplementary Fig. 5b** and **Supplementary Protocol**), and we produced milligram quantities of cNW11 that was >95% monomeric. Moreover, through multimerization we created an array of higher molecular weight circularized species and used these species to assemble larger nanodiscs (up to 80 nm in diameter) of well-defined circular and polygonal shapes (**Supplementary Figs. 5–7** and **Supplementary Note 2**).

Comparisons of proton relaxation rates of lipid resonances in empty cNW9 and conventional MSP1D1ΔH5 nanodiscs[4] indicated that more restriction is imposed on the lipids inside cNW9 by the covalently circularized belt protein than inside open MSP1D1ΔH5 nanodiscs (**Supplementary Fig. 8**). This could partially explain the enhanced thermal stability of circularized nanodiscs as compared to that of conventional nanodiscs (**Supplementary Fig. 9**). Covalent circularization also enhances the proteolytic stability of nanodiscs (**Supplementary Fig. 10**).

We next prepared labeled [U-$^{2}$H,$^{15}$N] VDAC-1 in cNW9 and cNW11 nanodiscs in order to incorporate one or two copies of the channel, respectively, and we recorded 2D $^{1}$H-$^{15}$N TROSY HSQC spectra at 45 °C (**Fig. 2a–d** and **Supplementary Fig. 11**). Earlier preparations with open nanodiscs resulted in undefined numbers of embedded VDAC-1 molecules, yielding inconsistent NMR spectra due to sample heterogeneity[5]. Our new data exhibit

[1]Department of Biological Chemistry and Molecular Pharmacology, Harvard Medical School, Boston, Massachusetts, USA. [2]Department of Cell Biology, Harvard Medical School, Boston, Massachusetts, USA. [3]Department of Biochemistry, University of Zurich, Zurich, Switzerland. [4]Department of Chemistry and Institute for Advanced Study, Technische Universität München and Helmholtz Centre Munich, Munich, Germany. [5]Present address: Rockefeller University, New York, New York, USA. Correspondence should be addressed to G.W. (gerhard_wagner@hms.harvard.edu).

RECEIVED 25 MARCH; ACCEPTED 19 OCTOBER; PUBLISHED ONLINE 21 NOVEMBER 2016; DOI:10.1038/NMETH.4079

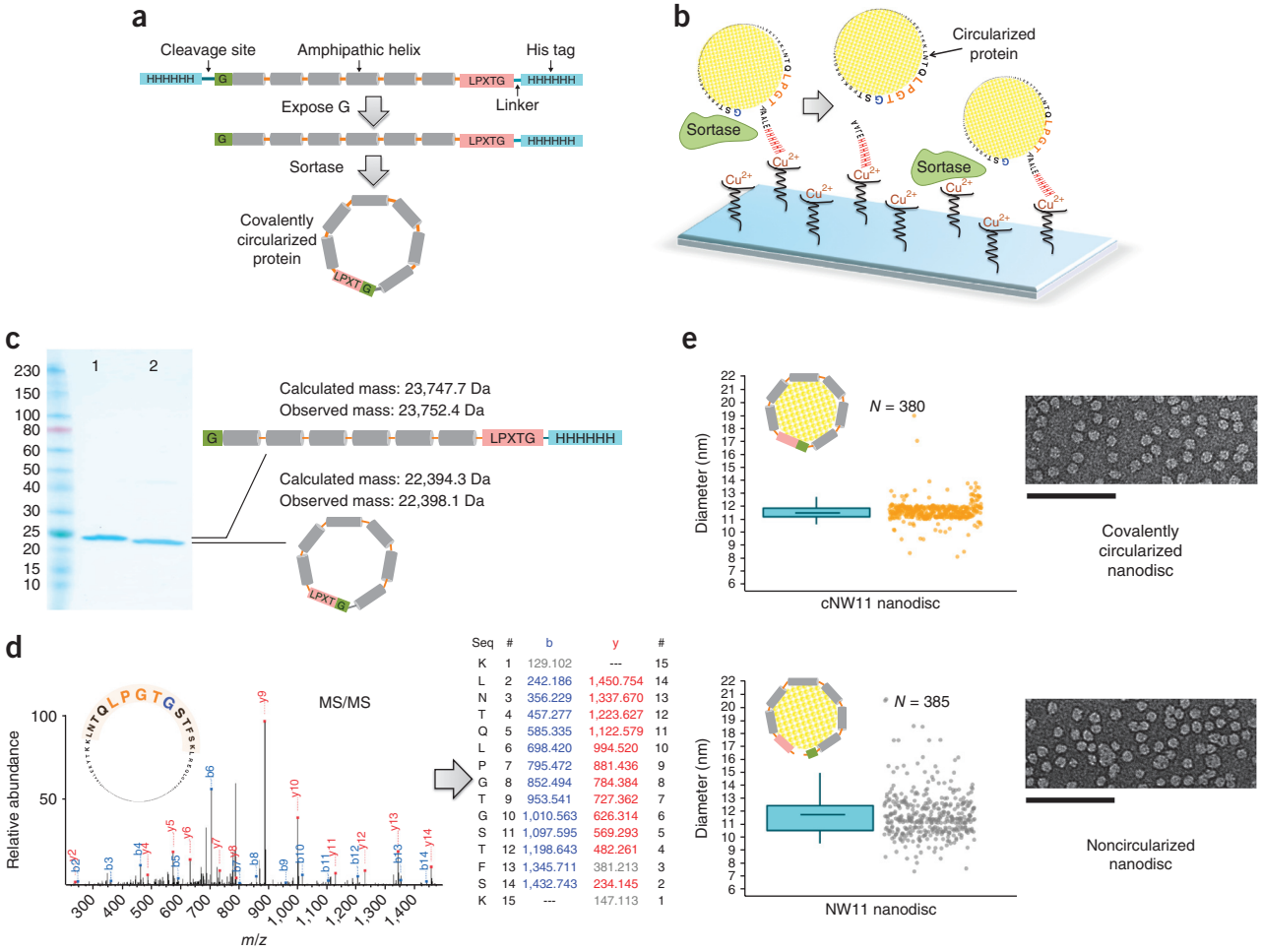


**Figure 1** | Producing covalently circularized NW11 and nanodiscs. (**a**) A general outline of the constructs that are used for making covalently circularized nanodiscs. Glycine (G) and LPXTG at the N and C termini are needed for linkage by sortase. (**b**) Outline of the procedure for creating circularized proteins over a $Cu^{2+}$ chip. Immobilizing NW11 on the $Cu^{2+}$ chip via a $His_6$ tag reduces the chances for head-to-tail linkage of two neighboring NW11 molecules and offers a quick reaction time. (**c**) SDS–PAGE analysis of NW11 before (lane 1) and after (lane 2) circularization. (**d**) MS/MS spectrum of a tryptic peptide of cNW11 confirming the ligation of the N-terminal residues (GSTFSK) to the C-terminal LPGTG motif. The b and y ions that were identified in the MS/MS spectrum are highlighted in blue and red, respectively. MS/MS and intact mass data for other NWs constructs (cNW9, cNW30 and cNW50) are provided in **Supplementary Table 1** and **Supplementary Figures 1–3**. Seq, sequence; gray indicates values not observed. (**e**) Diameter distribution based on negative-stain EM observations for nanodiscs made using circularized NW11 (top) and noncircularized NW11 (bottom) and representative negative-stain EM images. In the box-and-whisker plots, center lines show the mean; box limits indicate the 25$^{th}$ and 75$^{th}$ percentiles; whiskers go down to the 5$^{th}$ percentile and up to 95$^{th}$ percentile. The numbers of analyzed particles (*N*) are indicated in the figures. Raw data (jittered along *x*-axis for clarity) are shown next to their representative plot. Scale bars, 100 nm.

enhanced signal intensities and spectral resolution compared with those of previously reported NMR spectra of VDAC-1 in nanodiscs[5]. The $^{1}H$-$^{15}N$-TROSY HSQC spectra recorded for labeled [U-$^{2}H$,$^{15}N$] VDAC-1 are substantially different between cNW9 and cNW11, suggesting conformational differences and/or intermolecular contacts between the monomer and dimer forms of membrane-embedded VDAC-1. These experiments demonstrate the power of the cND approach to control the oligomeric state of dynamically interacting proteins for structural studies. Moreover, the observed stability and quality of NMR spectra of VDAC-1 in cNDs at 45 °C are dramatically better than obtained for VDAC-1 in nanodiscs formed with linear MSPs (**Supplementary Fig. 12**); and this enhanced stability and quality will greatly facilitate NMR assignments of VDAC-1.

We next acquired a $^{1}H$-$^{15}N$-TROSY HSQC spectrum of a $^{15}N$-labeled, signaling-competent variant of rat neurotensin receptor 1 (NTR1) in cNW9 nanodiscs (**Fig. 2e**,**f**). The cND sample was stable at 45 °C for longer than 10 d. We tested binding of a heterotrimeric G protein composed of $G\alpha_{i1}$, $G\beta_1$ and $G\gamma_1$ to cND-embedded NTR1, and this resulted in numerous spectral changes (**Fig. 2f**). The integrity of the cNW9 nanodiscs was not affected, even though the G protein was added with a small amount of DDM (the final DDM concentration was less than 10% of its critical micellar concentration (CMC)). We believe that cNDs will greatly facilitate the study of different dynamic events upon ligand binding in a near-native membrane environment, which may be critical for understanding the G-protein-coupled receptor (GPCR) mediated signal transduction process.

Next, we used the cNW50 nanodiscs as model membranes to study the question of how simple nonenveloped viruses transfer their genomes across membranes to initiate infection.

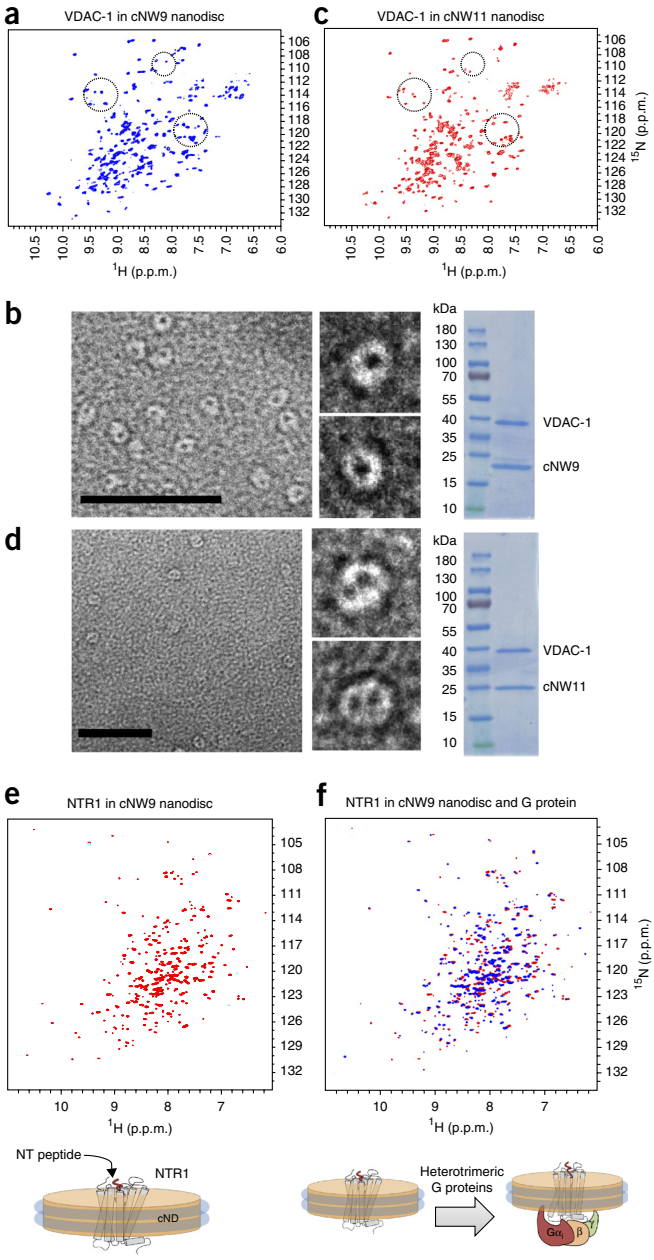


**Figure 2** | Analysis of membrane proteins in nanodiscs of different sizes. (**a**) 2D $^{1}$H-$^{15}$N-TROSY HSQC spectrum of monomeric labeled [U-$^{2}$H,$^{15}$N] VDAC-1 in cNW9 nanodiscs. p.p.m., parts per million. (**b**) Representative image of negatively stained cNW9 nanodiscs containing single VDAC-1 channel. The stain-filled channels appear as dark spots inside the nanodisc. Right, SDS–PAGE analysis of cNW9 nanodiscs containing VDAC-1. (**c**) 2D $^{1}$H-$^{15}$N-TROSY HSQC spectrum of dimeric labeled [U-$^{2}$H,$^{15}$N] VDAC-1 in cNW11 nanodiscs. (**d**) Representative image of negatively stained cNW11 nanodiscs containing two VDAC-1 channels. Right, SDS–PAGE analysis of cNW11 nanodiscs containing VDAC-1. (**e**) $^{1}$H-$^{15}$N-TROSY HSQC spectrum of 40 μM $^{15}$N-labeled NTR1 in cNW9 nanodisc acquired at 45 °C on a Bruker 800 MHz spectrometer. Bottom, cartoon representation of NTR1 in cNW9 nanodisc. (**f**) Superimposed $^{1}$H-$^{15}$N-TROSY HSQC spectra of 40 μM $^{15}$N-labeled NTR1 in cNW9 nanodisc before (red) and after (blue) addition of purified heterotrimeric G protein composed of $G\alpha_{i1}$, $G\beta_1$ and $G\gamma_1$. Bottom, cartoon representation of NTR1 in cNW9 nanodisc after the addition of heterotrimeric G protein. Scale bars, 50 nm (**b**,**d**).

Unlike enveloped viruses, nonenveloped viruses lack an external membrane, and the delivery of their genome into cells requires translocation across a membrane to gain access to the inside of the host cell[10,11]. Although there are now several model systems being used to study this process, the mechanism of genome translocation remains poorly understood[12], and a more detailed structural analysis of the membrane-associated forms of the cell-entry intermediates is required. So far, mechanistic insights have been limited, due in part to technical difficulties involved in direct visualization of viral gene delivery and size heterogeneity of liposomes.

Poliovirus (~30-nm diameter) is the prototype member of the enterovirus genus of the picornavirus family, which are positive-sense, single-stranded RNA viruses with ~7,500-base genomes enclosed by an icosahedral capsid, and they lack an envelope[13]. Viral infection is mediated by a specific receptor, CD155 (also known as the poliovirus receptor, PVR)[14]. Upon raising the temperature from 4 °C to 37 °C, the receptor catalyzes a conformational rearrangement and expansion of the virus particle. The expanded virus is then endocytosed by a noncanonical, actin-independent pathway[15], and the RNA is released across the endosomal membrane. The 50-nm cNW50 nanodisc is sufficiently large to accommodate multiple CD155 copies and has enough surface area to act as a surrogate membrane for the RNA-translocation complex during viral uncoating (**Fig. 3a**).

Similar to studies that used liposomes[16–18], cNW50 nanodiscs containing lipids derivatized with a nitrilotriacetate (NTA) nickel-chelating head group were generated and functionalized with the His-tagged CD155 ectodomain. The receptor-decorated nanodiscs were incubated with poliovirus for 5 min at 4 °C. The complex was then heated to 37 °C for 15 min to initiate receptor-mediated viral uncoating (**Fig. 3b**). Negative-stain EM confirmed virus binding to the CD155-decorated nanodiscs and subsequent insertion of viral components into and across the membrane (**Fig. 3c**). Additionally, the negative-stain EM images indicated that the virus started to form a pore in the nanodisc. To obtain a view of the molecular interactions involved in the RNA-translocation complex as well as to elucidate in more detail the formation of a pore, we conducted cryo-EM studies. **Figure 3d** and **Supplementary Figure 13** show the dark RNA-filled virus next to the slightly larger cNW50 nanodisc. The nanodisc is tilted in **Figure 3e** and tethered to the virus in **Figure 3f**. We visualized the formation of a putative pore inside the nanodiscs (**Fig. 3g**,**h**), through which the virus ejects its RNA. The identities of the pore-forming proteins are currently being determined.

The use of cNW50 nanodiscs greatly facilitates cryo-EM imaging as compared to the use of liposomes because the nanodiscs are more homogenous in size and shape, and they allow for the use of a thinner ice layer. Also, RNA can be visualized more easily in the absence of large liposomal membranes. In order to reduce complexity even further, we used cNW30 nanodiscs (~15 nm) decorated with CD155. Surprisingly, the virus also tethers to this smaller nanodisc (**Fig. 3i**) and ejects RNA, leaving an empty viral capsid behind (**Fig. 3j** and **Supplementary Fig. 14**). 3D reconstruction of these complexes will be challenging and is beyond the scope of this study. However, the quality of the data collected on the virus–nanodisc complexes represents a substantial improvement over data previously used to obtain low-resolution structural models of the translocation complex using the receptor-decorated liposome model[19].

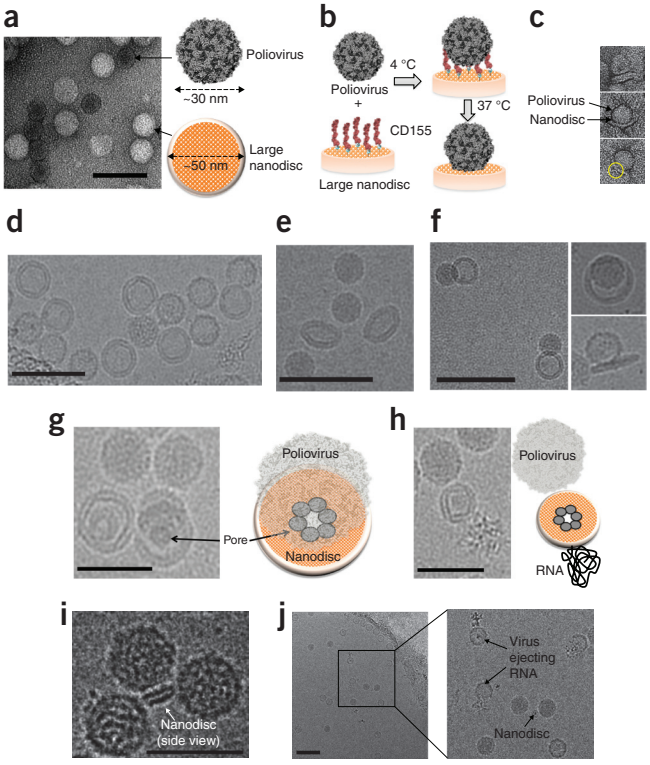


**Figure 3** | Poliovirus interactions with cNDs containing the CD155 receptor. (**a**) Negative-stain EM of 50-nm circularized nanodiscs plus poliovirus. A control (nanodiscs without CD155) is shown to illustrate the relative dimensions of the 30-nm poliovirus and the 50-nm nanodisc. (**b**) Outline of the procedure used to initiate poliovirus interaction with nanodiscs decorated with CD155. (**c**) Three negative-stain EM images showing individual viruses tethered to nanodiscs. The yellow circle (bottom) indicates potential pore formation. (**d**) Cryo-EM image of 50-nm nanodiscs plus poliovirus. (**e**) Cryo-EM image showing a tilted view of 50-nm nanodisc. (**f**) Cryo-EM images showing individual viruses tethered to nanodiscs. (**g**,**h**) Cryo-EM images showing the creation of a putative pore in the nanodisc by the poliovirus. Drawings to the right illustrate this process. (**i**) Cryo-EM image showing three viral particles around a 15-nm nanodisc. (**j**) Cryo-EM image showing individual viruses ejecting RNA after incubation with CD155-decorated 15-nm nanodiscs. Scale bars, 100 nm (**a**,**d**–**f**,**j**) and 50 nm (**g**–**i**).

In conclusion, we have demonstrated the construction of covalently circularized nanodiscs with a wide range of geometric shapes and sizes. The ability to make stable cNDs at multiple defined sizes up to 80-nm diameters provides tools to tightly embed much larger membrane proteins or their intramembrane and extramembrane complexes than previous nanodisc systems have allowed. Moreover, we have shown that the covalently circularizable scaffold proteins produce nanodiscs with high homogeneity in size and shape and with significantly improved stability compared with that of noncircularized forms, which should greatly facilitate their use for NMR and cryo-EM studies. We have demonstrated the utility of this model system to probe an outstanding question in the field of virology, and we believe that the system will similarly enable the structural and functional study of other large protein and membrane complexes.

## METHODS

Methods, including statements of data availability and any associated accession codes and references, are available in the online version of the paper.

*Note: Any Supplementary Information and Source Data files are available in the online version of the paper.*


### ACKNOWLEDGMENTS

The authors thank T. Raschle for his early contribution to this work and H. Chou, H. Arthanari and J. Ziarek for helpful discussions. The authors gratefully acknowledge the use of the services of the Taplin Mass Spectrometry Facility and the Center of Macromolecular Interactions (CMI). Addgene plasmid no. 75144 was a gift from D. Liu (Department of Chemistry and Chemical Biology, Harvard University, Cambridge, Massachusetts, USA). This work was supported by NIH grant 32GM113406 to M.L.N.; grant AI20566 to J.M.H.; and grants GM047467, GM075879 and AI037581 to G.W. G.W., A.P. and F.H. are supported by the Human Frontiers Science program. D.B. acknowledges support from the HHMI as a Gilliam Fellow. F.H. acknowledges support from the TUM Institute for Advanced Study cofunded by the European Commission as well as from the CIPSM excellence cluster and the DFG (SFB1035).


### AUTHOR CONTRIBUTIONS

The project was conceived by M.L.N. and G.W. Experiments were designed by M.L.N., D.B., G.W., M.S. and J.M.H. Experiments were carried out by M.L.N., D.B., M.S., Z.J.S., S.G. and S.H. The manuscript was written by M.L.N. and G.W. T.W., J.M.H., D.B., F.H., A.P. and S.G. contributed to discussions and editing of the manuscript.

### COMPETING FINANCIAL INTERESTS

The authors declare competing financial interests: details are available in the online version of the paper.




1. Bayburt, T.H., Carlson, J.W. & Sligar, S.G. *J. Struct. Biol.* **123**, 37–44 (1998).
2. Bayburt, T.H., Grinkova, Y.V. & Sligar, S.G. *Nano Lett.* **2**, 853–856 (2002).
3. Ritchie, T.K. *et al. Methods Enzymol.* **464**, 211–231 (2009).
4. Hagn, F., Etzkorn, M., Raschle, T. & Wagner, G. *J. Am. Chem. Soc.* **135**, 1919–1925 (2013).
5. Raschle, T. *et al. J. Am. Chem. Soc.* **131**, 17777–17779 (2009).
6. Grinkova, Y.V., Denisov, I.G. & Sligar, S.G. *Protein Eng. Des. Sel.* **23**, 843–848 (2010).
7. Raschle, T., Hiller, S., Etzkorn, M. & Wagner, G. *Curr. Opin. Struct. Biol.* **20**, 471–479 (2010).
8. Antos, J.M. *et al. J. Biol. Chem.* **284**, 16028–16036 (2009).
9. Chen, I., Dorr, B.M. & Liu, D.R. *Proc. Natl. Acad. Sci. USA* **108**, 11399–11404 (2011).
10. Hogle, J.M. *Annu. Rev. Microbiol.* **56**, 677–702 (2002).
11. Tuthill, T.J., Groppelli, E., Hogle, J.M. & Rowlands, D.J. *Viruses* **343**, 43–89 (2010).
12. Marsh, M. & Helenius, A. *Cell* **124**, 729–740 (2006).
13. Racaniello, V.R. *Fields Virology* 6th edn. (eds. Knipe, D.M. & Howley, P.M.) 453–489 (Lippincott, Williams & Wilkens, 2013).
14. Mendelsohn, C.L., Wimmer, E. & Racaniello, V.R. *Cell* **56**, 855–865 (1989).
15. Brandenburg, B. *et al. PLoS Biol.* **5**, e183 (2007).
16. Tuthill, T.J., Bubeck, D., Rowlands, D.J. & Hogle, J.M. *J. Virol.* **80**, 172–180 (2006).
17. Bubeck, D., Filman, D.J. & Hogle, J.M. *Nat. Struct. Mol. Biol.* **12**, 615–618 (2005).
18. Strauss, M., Levy, H.C., Bostina, M., Filman, D.J. & Hogle, J.M. *J. Virol.* **87**, 3903–3914 (2013).
19. Strauss, M. *et al. J. Virol.* **89**, 4143–4157 (2015).

## ONLINE METHODS

We provide a **Supplementary Protocol** that includes detailed step-by-step instructions for the production of NWs proteins, circularization reaction and nanodisc assembly. Additionally, materials are available upon request (also see "Data availability").

**Expression of NW9, NW11, NW30 and NW50.** NW9, NW11, NW30 and NW50 (all in pET-28a) containing a tobacco etch virus (TEV) protease-cleavable N-terminal $His_6$ tag and a C-terminal sortase-cleavable $His_6$ tag were transformed into BL21-Gold (DE3) competent *Escherichia coli* cells (Agilent). 3L cell cultures were grown at 37 °C with agitation at 200 r.p.m. in Luria broth (LB) medium supplemented with 50 μg/ml kanamycin. Expression was induced at an $OD_{600}$ of 0.6 with 1 mM IPTG, and cells were grown for another 3 h at 37 °C (NW9 and NW11) or 16 h at 18 °C (NW30 and NW50). Cells were harvested by centrifugation (7,000 x *g*, 15 min, 4 °C), and cell pellets were stored at −80 °C.

**Purification of NW9 and NW11.** Pellets of cells expressing NW9 or NW11 were resuspended in lysis buffer (50 mM Tris–HCl, pH 8.0, 500 mM NaCl, 1% Triton X-100) and lysed by sonication on ice. Lysate was centrifuged (35,000 × *g*, 50 min, 4 °C), and the supernatant was loaded onto an $Ni^{2+}$-NTA column. The column was washed with lysis buffer then with buffer A (50 mM Tris, pH 8.0, 500 mM NaCl). To recover additional protein from the insoluble fractions, the pellets recovered from lysate centrifugation were dissolved in denaturing buffer (50 mM Tris, pH 8.0, 500 mM NaCl, 6 M guanidine hydrochloride), centrifuged (35,000 × *g*, 50 min, 4 °C), and the supernatant was applied to the same $Ni^{2+}$-NTA column containing bound protein from the soluble fraction. The column was washed with denaturing buffer, and NW9 and NW11 were refolded on column with 10 column volumes (CV) buffer A. Resin was then washed with 10 CV of the following buffers: buffer A + 1% Triton X-100, buffer A + 50 mM sodium cholate, buffer A, and buffer A + 20 mM imidazole. Proteins were eluted with buffer A + 500 mM imidazole, TEV ($His_6$ tagged; produced in house) was added to cleave the N-terminal $His_6$ tag, and the samples were dialyzed against 50 mM Tris–HCl, pH 8.0, 100 mM NaCl, 1 mM EDTA, 2 mM DTT at 4 °C for 16 h. NW9 and NW11 (still containing a C-terminal $His_6$ tag) were exchanged into nanodisc-assembly buffer (50 mM Tris–HCl, pH 8.0, 500 mM NaCl, 0.02% $NaN_3$) using Centricon concentrators (10 kDa MW cutoff, Millipore).

**Purification of NW30 and NW50.** NW30 and NW50 were purified under denaturing conditions and refolded as follows. Pellets of cells expressing NW30 or NW50 were resuspended in denaturing lysis buffer (50 mM Tris–HCl, pH 8.0, 500 mM NaCl, 6 M guanidine hydrochloride) and lysed by sonication on ice. Lysate was centrifuged (35,000 × *g*, 50 min, 4 °C), and the supernatant was loaded onto a $Ni^{2+}$-NTA column. Resin was washed with 10 CV of denaturing lysis buffer to remove unbound proteins, and NW30 and NW50 were refolded on column with 10 CV buffer A (50 mM Tris–HCl, pH 8.0, 500 mM NaCl). Resin was washed with 10 CV of the following buffers: buffer A + 1% Triton X-100, buffer A + 50 mM sodium cholate, buffer A, and buffer A + 20 mM imidazole. Proteins were eluted with buffer A + 500 mM imidazole, TEV protease was added to cleave the N-terminal $His_6$ tag, and samples were dialyzed against 50 mM Tris, pH 8.0, 100 mM NaCl, 1 mM EDTA, 2 mM DTT at 4 °C for 16 h. NW30 and NW50 (still containing a C-terminal $His_6$ tag) were further purified by size exclusion chromatography (SEC; Superdex 200 16/60, GE Healthcare, equilibrated in 20 mM Tris–HCl, pH 7.5, 500 mM NaCl, 50 mM sodium cholate, 0.5 mM EDTA). SEC fractions containing NW30 and NW50 were further purified over $Ni^{2+}$-NTA resin to remove truncation products (which lack a C-terminal $His_6$ tag). Purified proteins were exchanged into nanodisc-assembly buffer (50 mM Tris–HCl, pH 8.0, 500 mM NaCl, 0.02% $NaN_3$) using Centricon concentrators (30 kDa MW cutoff, Millipore).

**Membrane scaffold protein circularization.** A 50 mL reaction was prepared with 10 μM NWs and 5 μM (final concentrations) freshly made evolved sortase (Addgene plasmid no. 75144, a gift from D. Liu, Harvard University) in 300 mM Tris–HCl, pH 7.5, 150 mM NaCl, and 10 mM $CaCl_2$. The reaction was incubated at 37 °C for 3–4 h or at 4 °C overnight with gentle shaking on a rotating platform. A covalent sortase inhibitor AAEK2 (ref. 20) was added to a concentration of 500 μM, and the solution was incubated for another 30 min at room temperature with gentle shaking. Proteins that did not undergo circularization were removed by binding to a $Ni^{2+}$-NTA column. Circularized NWs (cNWs) were further purified by size-exclusion chromatography (Superdex 75 16/60) equilibrated in buffer containing 20 mM Tris–HCl, pH 7.5, 500 mM NaCl containing 50 mM sodium cholate or 1 mM dodecyl-β-D-maltoside (DDM). Purified protein was exchanged into buffer $A_{ix}$ (20 mM Tris, pH 8.2, 1 mM DDM) using centricon concentrators (10 kDa MW cutoff, Millipore) and was then applied to a Resource Q column equilibrated with the same buffer (buffer $A_{ix}$). A linear salt gradient from 0–60% buffer $B_{ix}$ (20 mM Tris, pH 8.2, 1 mM DDM, 1 M NaCl) was applied. Circularized proteins were eluted around 150–200 mM NaCl.

**Reconstitution of cNW11, cNW30 and cNW50 nanodiscs.** cNWs:lipid ratios of 1:60, 1:75, 1:1,000 and 1:4,000 were used to assemble cNW9, cNW11, cNW30 and cNW50 nanodiscs, respectively. Lipids (POPC:POPG, 3:2; solubilized in sodium cholate) and cNWs were incubated on ice for 1 h. After incubation, sodium cholate was removed by incubation with Bio-beads SM-2 (Bio-Rad) for 1 h on ice followed by incubation overnight at 4 °C. The nanodisc preparations were filtered through 0.22 μm nitrocellulose-filter tubes to remove the Bio-beads. The nanodisc preparations were further purified by size-exclusion chromatography while monitoring the absorbance at 280 nm on a Superdex 200 10 × 300 column (for cNW9 and cNW11 nanodiscs) or Superose 6 10/300 column (for cNW30 and cNW50 nanodiscs) equilibrated in 20 mM Tris–HCl, pH 7.5, 100 mM NaCl, 0.5 mM EDTA. Fractions corresponding to the size of each nanodisc were collected and concentrated. The purity of nanodisc preparations was assessed using SDS–PAGE.

***In vitro* reconstitution of VDAC-1 into POPC–POPG or DMPC–DMPG nanodiscs.** To assemble VDAC-1 into POPC–POPG nanodiscs, 15 μM of VDAC-1, 150 μM of cNW11 and 8.5 mM lipids (POPC:POPG, 3:2; solubilized in sodium cholate) were incubated over ice for 1 h. To assemble monomeric VDAC-1 into DMPC–DMPG nanodiscs for NMR experiments, 25 μM of VDAC-1, 175 μM of cNW9 and 9.5 mM lipids (DMPC:DMPG, 3:1) were incubated for 1 h at room temperature. To assemble

dimeric VDAC-1 into DMPC–DMPG nanodiscs for NMR experiments, 79 μM of VDAC-1, 75 μM of cNW11 and 3.75 mM lipids (DMPC:DMPG, 3:1) were incubated for 1 h at room temperature. After incubation, detergents were removed by the addition of Bio-beads SM-2 (Bio-Rad) and incubation for 1 h on ice followed by overnight incubation at 4 °C (POPC–POPG nanodiscs) or overnight incubation at room temperature (DMPC–DMPG nanodiscs). The nanodisc preparation was filtered through 0.22 μm nitrocellulose-filter tubes to remove the Bio-beads. To remove the VDAC-free nanodiscs, the sample was mixed with $Ni^{2+}$-NTA resin for 1 h at 4 °C. The resin bed volume was equal to the assembly mixture. The resin was washed with buffer E (20 mM Tris–HCl, pH 8.0, 0.1 M NaCl, 20 mM imidazole). Nanodiscs containing VDAC were eluted with buffer E containing 0.5 M imidazole. The nanodisc preparation was further purified by size-exclusion chromatography while monitoring the absorbance at 280 nm on a Superdex 200 10 × 300 or a 16/60 Superdex 200 prep grade columns (GE Healthcare) equilibrated in buffer F (20 mM sodium phosphate, 50 mM NaCl, 5 mM DTT, 1 mM EDTA, pH 7.0). Fractions corresponding to the size of the VDAC–nanodisc complex were collected and concentrated. The purity of VDAC-containing nanodiscs was assessed using SDS–PAGE.

**Production of NTR1 and reconstitution into DMPC–DMPG nanodiscs.** Expression and the purification of a signaling-competent, thermo-stabilized variant of rat neurotensin receptor 1 (termed HTGH4) were performed as described previously[21,22] with some modifications. Briefly, the full-length fusion protein consisting of maltose-binding protein (MBP), followed by a His tag, a 3C protease recognition site, NTR1, a second 3C protease recognition site, thioredoxin (TrxA), and a His tag at the C terminus was purified by $Ni^{2+}$ affinity chromatography. The purified full-length fusion protein was immediately incorporated into DMPC:DMPG (3:1) cNW9 nanodiscs. The assembled nanodiscs were subjected to $Ni^{2+}$ affinity chromatography to remove empty nanodiscs from the receptor-containing nanodiscs using the His tag of the fusion protein. The receptor-containing nanodiscs were further purified by size-exclusion chromatography followed by incubation with resin decorated with 3C protease-cleavable neurotensin peptide (pD-NT) to enrich for nanodiscs containing correctly folded receptors. Next, the pD-NT column was incubated for 2 h with His-tagged 3C protease (produced in house). The eluted proteins (neurotensin-bound NTR1 in nanodiscs, MBP, TrxA and 3C protease) were subjected to another $Ni^{2+}$ affinity chromatography followed by size-exclusion chromatography using a Superdex-200 10/300 column that was pre-equilibrated with running buffer containing 20 mM sodium phosphate, pH 6.9, 50 mM NaCl, 5 mM DTT, 1 mM EDTA.

Heterotrimeric G protein ($\alpha_{i1}\beta_1\gamma_1$) was expressed in Sf9 cells using a single baculovirus encoding all three subunits as previously described[22] and purified following a published procedure[23].

**Negative-stain electron microscopy.** Samples were prepared by conventional negative staining as described previously[24]. Briefly, 3.5 μl of nanodisc samples were adsorbed to glow-discharged, carbon-coated copper grids and stained with 0.75% (w/v) uranyl formate. All EM images (except images for VDAC-1 in cNW9 nanodiscs in **Supplementary Fig. 11**) were collected with a Philips CM10 electron microscope (FEI) equipped with a tungsten filament and operated at an acceleration voltage of 100 kV. Images were recorded with a Gatan 1 K × 1 K CCD camera (Gatan, Inc., Pleasanton, CA, USA). Using the EMAN software package[25], 9,258 particles were selected from 69 images of VDAC-1 in cNW9 nanodiscs (recorded at a magnification of 42,000×, defocus value of −1.5 μm) and classified into 150 classes.

**NMR spectroscopy.** Labeled [U-$^{2}$H,$^{15}$N] VDAC-1 in DMPC:DMPG (3:1) nanodiscs (611 μM and 500 μM of VDAC1 in cNW9 and cNW11 nanodiscs, respectively) were prepared as described above in NMR buffer (20 mM $NaPO_4$, 50 mM NaCl, 5 mM DTT, 1 mM EDTA, pH 7.0, 6% $D_2O$). $^{15}$N-TROSY HSQC data were collected at 45 °C on a Bruker 800-MHz spectrometer equipped with a TXO cryogenic probe. Data for VDAC-1 in cNW9 and cNW11 nanodiscs were acquired with 48 and 96 scans, respectively, and 128 complex points in the $^{15}$N-indirect dimension.

The $^{15}$N-TROSY HSQC spectrum of 40 μM $^{15}$N-labeled NTR1 in cNW9 nanodiscs was acquired at 45 °C on a Bruker 800-MHz spectrometer. Data were collected with 2,048 scans per FID and 36 nonuniformly sampled $^{15}$N-dimension complex points (maximum point of 64). The $^{15}$N-dimension time domain data were reconstructed with hmsIST[26] and processed by NMRPipe software programs[27].

**Cryo-electron microscopy.** A 3.5 μl droplet of the poliovirus–nanodisc complex was loaded onto a glow-discharged holey carbon grid (Protochips, Morrisville, North Carolina). Excess liquid was removed from the grid surface before it was rapidly plunged into liquid ethane. Grids were transferred into an FEI Polara electron microscope operating at an acceleration voltage of 300 kV. Micrographs were acquired on a K2 Summit camera (Gatan, Pleasanton, California) in super-resolution mode using SerialEM[28], whereby 25 frames were collected for a total dose of 30 electrons per square Ångstrom. These frames were aligned and averaged using motioncorr[29].

**Statistics.** We graphically displayed the distribution of diameters of the circularized and uncircularized nanodiscs using box-and-whisker plots (**Fig. 1** and **Supplementary Fig. 4**) and compared the variances using a variance ratio test. Diameter measurements were done with ImageJ software[30].

**Data availability.** Expression plasmids have been deposited at and will be available from the Dana Farber/Harvard Cancer Center (DF/HCC) plasmid depository (http://dnaseq.med.harvard.edu/) with the following codes: NW9, HsCD00483424; NW11, HsCD00483425; NW30, HsCD00483426; and NW50, HsCD00483427. Source data for **Figure 1** and **Supplementary Figures 4**, **8** and **9** are available with the paper online.


20. Maresso, A.W. *et al. J. Biol. Chem.* **282**, 23129–23139 (2007).
21. Egloff, P. *et al. Proc. Natl. Acad. Sci. USA* **111**, E655–E662 (2014).
22. Egloff, P., Deluigi, M., Heine, P., Balada, S. & Plückthun, A. *Protein Expr. Purif.* **108**, 106–114 (2015).
23. Rasmussen, S.G. *et al. Nature* **477**, 549–555 (2011).
24. Ohi, M., Li, Y., Cheng, Y. & Walz, T. *Biol. Proced. Online* **6**, 23–34 (2004).
25. Tang, G. *et al. J. Struct. Biol.* **157**, 38–46 (2007).
26. Hyberts, S.G., Milbradt, A.G., Wagner, A.B., Arthanari, H. & Wagner, G. *J. Biomol. NMR* **52**, 315–327 (2012).
27. Delaglio, F. *et al. J. Biomol. NMR* **6**, 277–293 (1995).
28. Mastronarde, D.N. *J. Struct. Biol.* **152**, 36–51 (2005).
29. Li, X., Grigorieff, N. & Cheng, Y. *J. Struct. Biol.* **172**, 407–412 (2010).
30. Schneider, C.A., Rasband, W.S. & Eliceiri, K.W. *Nat. Methods* **9**, 671–675 (2012).






doi:10.1038/nmeth.4079